

Atomic Scale Visualization of Vibrational Modes in Armchair Graphene Nanoribbon

Stefan Šćepanović, Diego López-Alcalá, José J. Baldoví, Alexander Vahl, and Abdou Hassanien*

Using scanning tunneling microscopy (STM) and inelastic tunneling spectroscopy, the low-frequency vibrational modes of a 7-atom wide armchair graphene nanoribbon (7-AGNR) is mapped. The inelastic tunneling channel is enhanced over the elastic one by a covalently bonded 7-AGNR to the apex of an STM tip. This setup has led to resonant inelastic tunneling between vibrational states of supported 7-GNR on Au(111) substrate and the states of the functionalized STM tip. The low-energy spectra reveal two localized peaks at the armchair edges with energies at ± 14 and ± 30 mV. The peaks are assigned to twice the energies of longitudinal compressive and shear-like modes of 7-AGNR, respectively. Remarkably, the well-separated peaks evolve rapidly into one broader peak toward the bulk of the ribbon due to scattering from substrate interactions. This suggests that edge state phonons are uniquely protected from the microenvironment and may have a profound effect on the transport properties of GNR devices.

attracted wide research interests due to their potential for electronic applications.^[1] Some of these interests stem from the fact that they are clean, 1D systems with properties that can be tailored using bottom-up technologies. For example, 7-AGNR can host topological states by either inline edge extension^[2] or seamless formation of a heterojunction with 9-AGNR.^[3] Moreover, AGNR can also be made magnetically active by either chemical attachment of radicals,^[4] zigzag edge extensions along the armchair sides,^[5] abstraction of hydrogen atoms,^[6] nonplanar distortion at termini,^[7] etc. The interplay between these structures and the electronic properties has been studied thoroughly by scanning tunneling microscopy (STM).^[8] However, for robust device functionality, it is important to also investigate the inelastic excitations which

limit current flow or cause dissipative process that leads to failure. To study the details of such dissipative processes and how they couple to charge transport, the inelastic tunneling microscopy offers a great tool to visualize the spatial dependence down to the atomic scale. Unfortunately, as conventional STM measurements are mostly due to elastic processes, it is very difficult to probe low-level inelastic excitations such as vibrational eigenstates, especially on supported molecules,^[9] as phonons may also interact with electrons from the metal substrate. This interaction tends to reduce the lifetime of the vibrational modes, thus making it difficult to couple with tunneling electrons. As reported in earlier studies by J. van der Lit et al., low vibrational states are hidden under rather broad vibrational states of higher energies and are only visible at termini.^[10] For this reason, the scanning tunneling microscope tip must be functionalized^[11] to enhance the inelastic tunneling channel. Further and direct enhancement can be made, as in the current work, by matching the energy of tunneling electrons^[12] with the local vibrational modes of supported structures. When the tunneling electrons are in resonance with these local excitations, a maximum transfer of energy occurs, and peaks in the local density of states are clearly visible.^[13] In the current study, the tip is modified by chemically attaching 7-AGNR to the apex. The chemical attachment provides robust bonding, which is essential for carrying out both stable imaging and local spectroscopy for an extended period of time. The details of this process are published elsewhere^[12] and are briefly described in the sample preparation section. Peaks in the positive and negative biases are due to phonon emission

1. Introduction


Semiconducting armchair graphene nanoribbons, such as 7-atom wide armchair graphene nanoribbon (7-AGNR), have

S. Šćepanović, A. Hassanien
Jozef Stefan Institute
39 Jamova, 1000 Ljubljana, Slovenia
E-mail: abdou.hassanien@ijs.si

D. López-Alcalá, J. J. Baldoví
Instituto de Ciencia Molecular
Universitat de València
Catedrático José Beltrán 2, 46980 Paterna, Spain

A. Vahl
Leibniz-Institute for Plasma Science and Technology (INP)
Felix-Hausdorff-Str. 2, 17489 Greifswald, Germany

A. Vahl
Composite Materials
Kiel University
Kaiserstr. 2, 24143 Kiel, Germany

 The ORCID identification number(s) for the author(s) of this article can be found under <https://doi.org/10.1002/pssr.202500203>.

© 2025 The Author(s). physica status solidi (RRL) Rapid Research Letters published by Wiley-VCH GmbH. This is an open access article under the terms of the Creative Commons Attribution-NonCommercial-NoDerivs License, which permits use and distribution in any medium, provided the original work is properly cited, the use is non-commercial and no modifications or adaptations are made.

DOI: 10.1002/pssr.202500203

and absorption, respectively. Their symmetric behavior around zero bias illustrates a strong inelastic coupling between tip and sample vibrational states. These results show that edge phonons are unique and less scattered by substrate interaction than bulk phonons.

In the following sections, we present our studies on imaging with a functionalized tip, then we focus on probing the local vibrational modes and their spatial variations, especially in the vicinity of edges and termini. We demonstrate the localization of edge phonons by performing high-resolution inelastic tunneling spectroscopy (IETS) that shows a well-separated peaks only at these sites. We then discuss the mixing behavior of these vibrational states toward the bulk due to substrate interactions. We assign these phonons to the longitudinal compressive and shear-like modes, which are known to be omnipresent in all AGNR.^[14]

2. Sample Preparation and Measurements

Atomically clean 7-AGNRs were prepared by the usual two-step annealing process of commercially available molecular precursor 10,10'-dibromo-9,9'-bianthryl (DBBA) on Au(111).^[15] The detailed steps of sample purification and deposition on Au(111) substrates are published elsewhere.^[6] We use a commercial Joule-Thompson scanning tunneling microscope (JT-STM), which can be operated down to 1.6 K. High-quality images of 7-AGNR on Au(111) are obtained by scanning the samples in constant current mode. To visualize the charge density pattern and enhance the IETS, the STM tip was functionalized by chemically bonding 7-AGNR at the apex. The bonding procedure^[12] is performed on the dehydrogenated site, which is usually located at the zigzag terminus.^[6] Prior to vertical manipulations, the STM tip is coated with Au by controlled crashing within 1–2 nm on a clean area of Au(111). Next, we locate the tip at the terminus, and vertical manipulation is carried out by the approach-withdraw procedure with a maximum current set to 7 nA at –50 mV bias voltage. The successful manipulation occurs when the current abruptly increases above the set point. In order to test the origin of inelastic peaks, we carried out temperature dependence of tunneling spectroscopy at the same local position. The scanning tunneling spectroscopy (STS) was collected using the usual lock-in technique with modulations ranging from 50 μ V to 1 mV. Topographic images and dI/dV maps reveal a pattern of charge density modulations near the edges and termini of 7-AGNR. 2-D fast Fourier transform (FFT) processing was carried out on large-scale images showing peaks that coincide with half of the Fermi wavelength. We used WSxM software^[16] for FFT, plane correction, and smoothing the images, but without any major further processing.

3. Results and Discussions

In this study, we have utilized a functionalized STM probe, which was made by chemically bonding Au-coated W tip with 7-AGNR at the apex. This covalent bonding allowed us not only to achieve high-resolution imaging of charge density but also to tune the energy of tunneling electrons to align with the local vibrations of 7-AGNR/Au(111). When in resonance, the dI/dV

signal intensity is enhanced at onsets of the vibrational eigenstates, thus making it possible to selectively probe the inelastic tunneling channel at various locations.

Figure 1a displays a topographic image of 7-AGNR on Au(111). The nanoribbons align with the high symmetry axes of the Au(111) substrate, demonstrating epitaxial growth similar to our previous studies.^[6] After attaching 7-AGNR to the tip, the image is highly enhanced and more details are clearly visible, as shown in **Figure 1b**. Ripples are due to charge density modulations^[17] on the armchair lattice with a period of 0.37 nm, which coincide very well with half of the Fermi wavelength of the graphene lattice (Larger scale image together with its FFT can be seen in **Figure 1S**, Supporting Information. A larger view is shown in **Figure 1c**, where both 7 and 13-AGNR are present in our samples, which gave us the opportunity to conduct IETS measurements at different ribbon widths. The inset is a line profile along the blue line.

Next, we address the vibrational states and their spatial variations on various nanoribbons. **Figure 2a** displays a typical STS data with a small-scale energy window at selected locations, marked by colored dots, on an isolated 7-AGNR. The dI/dV spectra of the bulk states show symmetric peaks around zero bias with energies at ± 31 mV. Interestingly, each peak splits into two peaks as we approach the armchair edges as well as the termini. In order to identify the origin of these peaks, we have performed temperature dependence of dI/dV spectra at equivalent locations. Results are shown in **Figure 2b**. As the temperature increases, the peaks broaden and increase in intensity, which indicates that they originate from vibrational modes. In addition to thermal broadening, the large increase in linewidth at higher temperature can be attributed to reduced lifetime of phonon modes due to enhanced electron-phonon scattering from substrate interactions. This weakens the coupling between tunneling electrons and the vibrational states, which contribute profoundly to the observed broadening in the linewidth. At temperatures below 5 K, the IETS is significantly reduced to be visible in our dI/dV. This is most likely due to the relatively low phonon population at these temperatures. For this reason, higher resolution IETS may be achieved by decoupling GNR from the underlying substrate, for example, by using a buffer NaCl layer. Moreover, it is interesting to note that these vibrational modes are hidden in the conventional STS measurements due to inefficient coupling with tunneling electrons, as GNR/substrate interactions^[18] tend to reduce the lifetime of vibrational excitations.^[19] In some cases, they are only visible within a rather broader peak of edge states at termini.^[10] Other reports have shown that such vibrational states can also appear in transport measurements of graphene devices,^[20] which affects device performance, as well as sets an upper limit to current flow. In our case here, the tunneling with a functionalized 7-AGNR tip augments the tunneling electron density at onsets of twice the vibrational mode energies, $\pm 2\hbar\omega$, thus we attribute those peaks to the absorption and emission of phonons from supported AGNR, respectively (see **Figure 2S**, Supporting Information). Here, ω is the frequency of the phonon mode. The symmetric behavior of $2\hbar\omega$ around zero bias indicates an efficient coupling between the 7-AGNR-tip and the supported 7-AGNR phonons. Nevertheless, the observed peaks are relatively broad, even with a functionalized tip. This

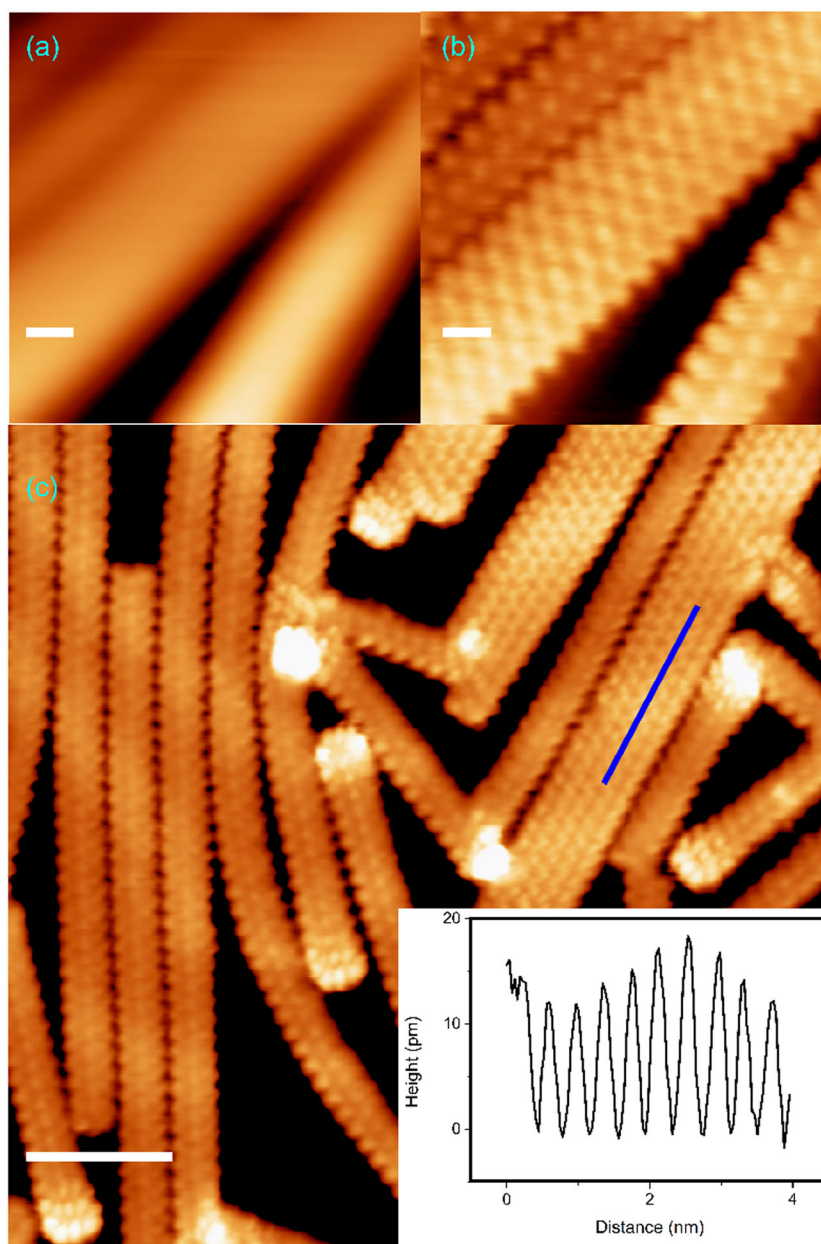


Figure 1. Topographic STM images of 7-AGNR on Au(111). The scanned area of a) is the same as in b) with Au-coated W tip and a 7-AGNR tip, respectively. The ripple in (b) is due to charge density modulation on the AGNR. c) is a larger view showing several 7-AGNRs, including some wider 13-AGNR. The inset is a line profile along the blue line. The scales in (a–c) are 0.5, 0.5, and 3 nm, respectively. The bias voltage is 300 mV, and the tunneling current is 100 pA.

broadening may be attributed to phonon scattering from states of the substrate and the positively charged AGNR on Au(111).

At edges and termini, two peaks in the IETS can be clearly identified at ± 12 and ± 19 mV. Earlier Raman spectroscopy of 7-AGNR on an insulating substrate^[14] has attributed low-frequency vibration, which occurs around $70\text{--}200\text{ cm}^{-1}$ (8.7–24.8 meV) to the longitudinal compressive mode (LCM). According to our density functional theory (DFT) calculations, this normal vibration mode corresponds to the compression/elongation of edge atoms in 7-AGNR at 130 cm^{-1} (16.1 meV)

(as shown in Figure 4). Another low-frequency mode around 270 cm^{-1} (33.5 meV), known as shear-like mode (SLM), is also omnipresent in AGNR. The study has shown that the frequency of SLM mode is related to the width of the ribbon and may also be affected by structural defects.^[21] So far, no STM study has reported the spatial variations of LCM and SLM due to inefficient coupling between tunneling electrons and the inelastic channels. Although the origin of well-resolved LCM and SLM peaks at the edges is not clear yet, the spatial dependence suggests less scattering at these locations. Interestingly, several theoretical studies

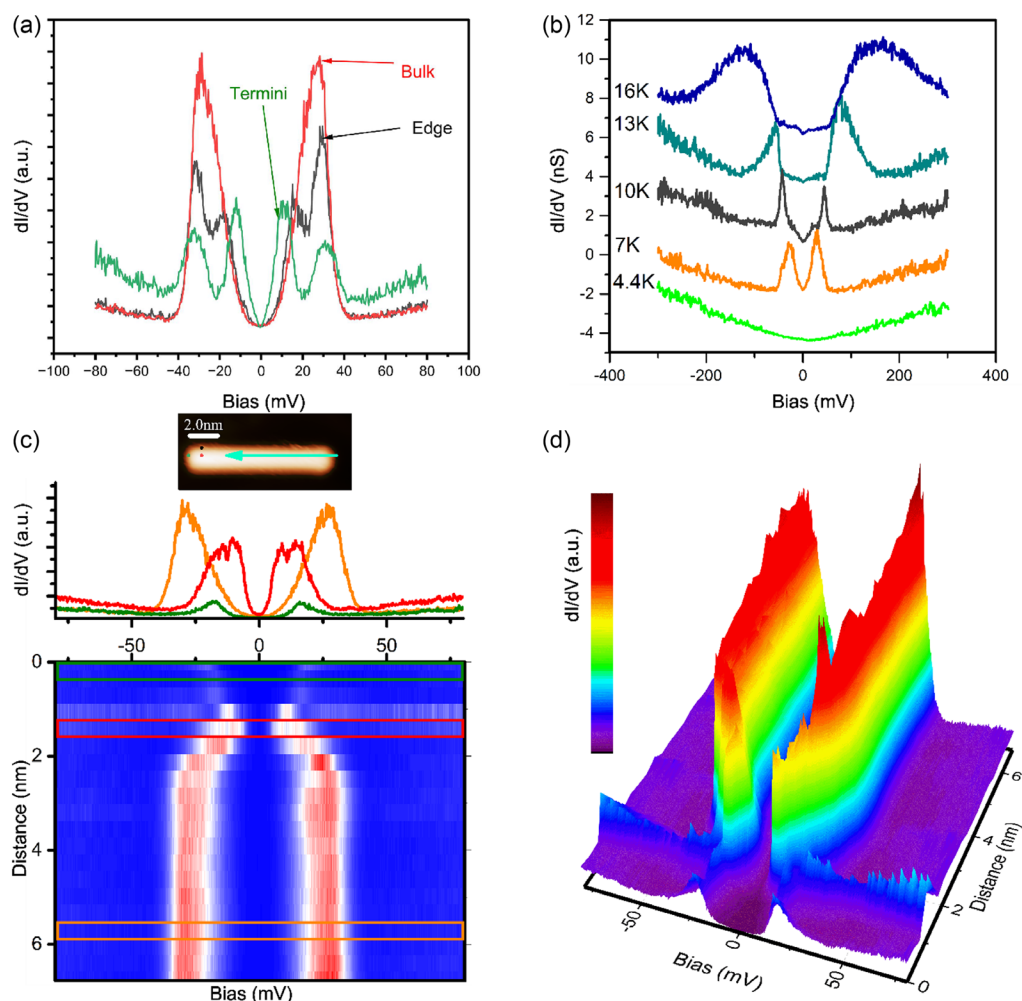


Figure 2. IETS on 7-AGNR. a) Comparison between IETS on 3 different locations. The peaks due to bulk states are more intense and broader than those at the edge and terminus. Splitting of this peak at edges and termini is most likely due to less coupling with substrate states. b) Temperature dependence shows peaks evolve broader and are enhanced as phonon populations increase with temperature. The curves are offset for better visibility. c) Spatial variation of IETS along bulk states. The green arrow in the inset shows the location of the dI/dV spectra. The selected spectra in the upper panel are taken at Au(111), termini, and 5 nm away and shown in the same colors with lines in the lower panel. d) is a 3D view of data in the lower panel of (c).

have pointed out that edge phonons of AGNR are more isolated^[22] from bulk phonons even in single-layer graphene.^[23] This indeed can explain the unique spatial behavior of localized peaks only at the edges. Our calculations on free-standing 7-AGNR didn't reveal such enhanced resolution at the edges. For this reason, we don't rule out the effect of substrate interactions. In future studies, it would be interesting to study these subtle details in the LCM and SLM with more elaborate theoretical calculations that take into account explicitly the interactions with the metallic substrate. The line profile in Figure 2c,d displays more details on the evolution of eigenstates of LCM along the bulk of the nanoribbon. The signal intensity is weaker at the termini and strengthens rapidly toward the bulk region.

We finally address the variation of LCM and SLM within a densely packed 7-AGNR. As the IETS signal changes rapidly in the vicinity of the edges, we performed high-resolution measurements perpendicular to the armchair edges. More specifically, the curves are spaced by 0.6 Å to follow closely the edge states

phonon and how they evolve into the bulk. Results are shown in Figure 3. The dI/dV profile across 6 nanoribbons is shown in Figure 3a,b with arrows in colors marking selected curves from two equivalent locations at the edge and the middle of two nanoribbons (see Figure 3c). Similar to the aforementioned results on individual nanoribbon, the spectra display two peaks at the edge that tend to merge into one broad peak toward the bulk of the ribbons. This peak broadening might be due to phonon scattering with other modes from the substrate. In earlier work,^[24] Yan et al. have shown that phonon mixing occurs in bilayer graphene due to inversion symmetry breaking, which allows anticrossing coupling. In our case, such an effect might also occur due to interaction with Au(111). At edges, the LCM and SLM modes are more resolved than in the bulk and can be identified with $\eta\omega$ equals half of the peaks at around ± 14 and ± 29.7 mV, respectively. These values are similar to the values obtained from Raman spectroscopy of 7-AGNR on an insulating substrate.^[14] It was argued that the LCM is ubiquitous for

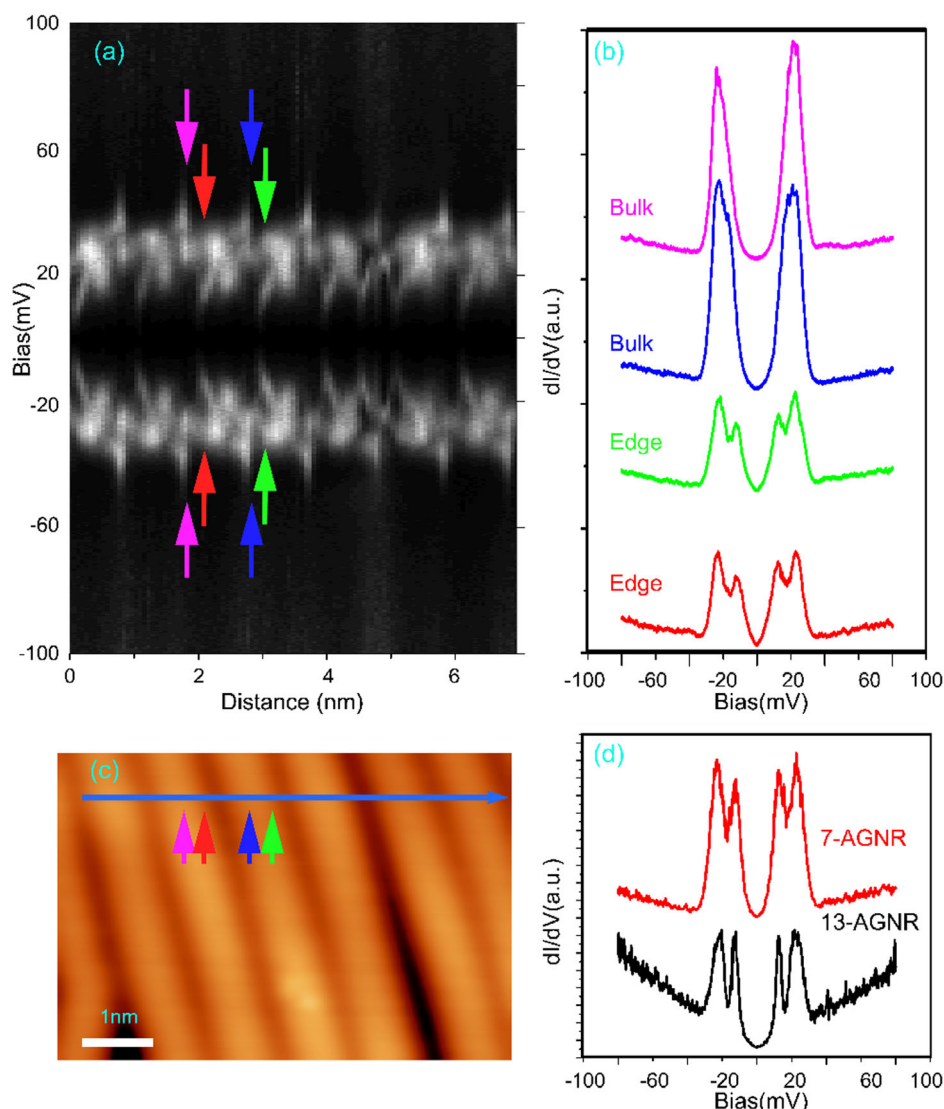


Figure 3. Evolution of edge state phonon into the bulk 7-AGNR. a) gray scale map of dI/dV taken at each 0.6 \AA to visualize the spatial variation of edge state across 6 nanoribbons. The arrows are marking edges in red and green, while the bulk are in magenta and blue colors. b) dI/dV spectra at the selected locations in (a). c) Line profile of dI/dV with arrow pointing at the position of measurements in (a,b). d) Comparison between the edge state of 7-AGNR and 13-AGNR.

all AGNR and shifts towards lower energies as the length of AGNR increases, especially for 5-AGNR. However, in our studies, due to substrate interactions, we haven't been able to address the length-dependent relationship of LCM frequency at this stage. Nevertheless, we can identify two low-frequency modes at the armchair edges that are reminiscent of LCM and SLM. For example, the peak at $\pm 29.7 \text{ mV}$ is clearly resolved at the edge and tends to broaden significantly toward the bulk region. This peak corresponds to twice the energy of SLM, which has been discussed by Ma et al.^[25] Figure 3d shows LCM and SLM for 7- and 13-AGNR taken at the edge. Again, the dI/dV spectra reveal similar values for LCM and SLM at both edges regardless of the width of the nanoribbon.^[14] This shows that phonons at edges are more protected from bulk phonons, and mixing between these two modes evolves toward the bulk of GNR.

This has been predicated theoretically in earlier works by several groups.^[26] Such phonon confinement is demonstrated in Figure 3a, where the signal changes rapidly within 1 \AA from the edge.

In Figure 4, we show the calculated displacement vectors for the LCM and SLM. According to our DFT calculations, LCM corresponds to an energy of $\approx 130 \text{ cm}^{-1}$, which is compatible with similar theoretical results at the same level of theory. This vibrational mode consists of the compression/elongation of the GNR in the direction of the C backbone (Figure 4a). Here, one can see that the magnitude of the displacement is accumulated at the edge atoms, whereas "bulk" atoms at the middle of the GNR are barely distorted in this normal mode of vibration. SLM corresponds to an energy of 263 cm^{-1} , which is in good agreement with previous theoretical results for 7-AGNR.^[21] This Raman

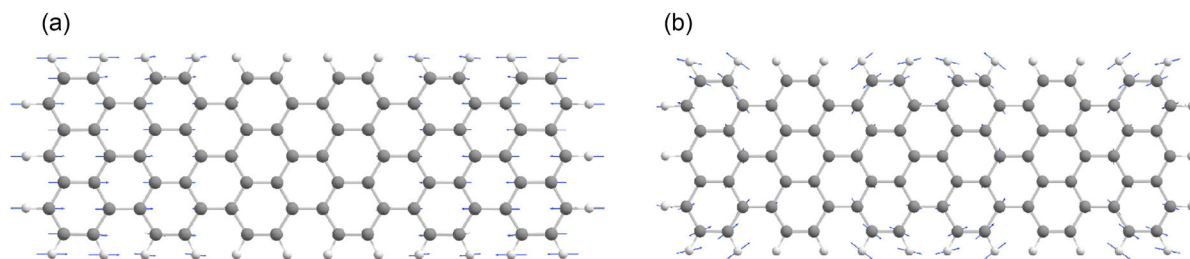


Figure 4. a) DFT-calculated displacement vectors for the LCM in a 7-AGNR. Arrows indicate the direction and magnitude of atomic displacements along the vibrational mode. b) Displacement vectors for the SLM, which involve atomic displacement of adjacent units sliding against each other.

active mode consists of the shear movement of the nanoribbon, where adjacent parts within the ribbon slide against each other parallel to the ribbon plane.

4. Conclusion

In summary, we have illustrated a straightforward method to probe the low-frequency vibrational state on AGNR using IETS with a functionalized STM tip. By utilizing 7-AGNR as a probe tip, the tunneling electrons are tuned in resonance with the vibrational mode of the supported nanoribbons. A strong coupling between these excitations is manifested as peaks in the dI/dV spectra at the onset of twice the vibrational eigenstates. We identify two vibrational modes that are more pronounced at the edges. The peaks are merged into one broader peak, which might be due to mixing or scattering of phonons by substrate interactions. Edge state phonons, however, are localized and less affected by substrate interactions.

Our DFT theoretical analysis performed on a free-standing 7-AGNR accurately captured the nature of LCM and SLM, but didn't take into account the substrate interaction, as this would require more elaborate and prohibitively expensive calculations beyond the scope of this work. In future studies, it would be of interest to perform a higher level of theory to study in detail the substrate interactions and how they affect the evolution of phonon modes away from edges and termini.

Finally, the sensitivity of this method to probe the vibrational modes, even on a metallic substrate, would be useful to directly visualize low-frequency modes in other graphene structures such as chiral GNRs and twisted bilayer graphene.

Supporting Information

Supporting Information is available from the Wiley Online Library or from the author.

Acknowledgements

This work was financially supported by the Slovenian Research Agency (ARIS) under Program No. P1-0099. D.L.A. and J.J.B. acknowledge the funding from the European Union (ERC-2021-StG 101042680 2D-SMARTIES) and Generalitat Valenciana (grant CIDEXG/2023/1).

Conflict of Interest

The authors declare no conflict of interest.

Data Availability Statement

The data that support the findings of this study are available from the corresponding author upon reasonable request.

Keywords

edge phonons, graphene nanoribbons, inelastic tunneling, scanning tunneling microscopy, vibrational modes

Received: May 26, 2025

Revised: July 31, 2025

Published online:

- [1] a) S. Lou, B. Lyu, X. Zhou, P. Shen, J. Chen, Z. Shi, *Quantum Front.* **2024**, 3, 3; b) S. Dutta, S. K. Pati, *J. Mater. Chem.* **2010**, 20, 8207; c) Z. Chen, A. Narita, K. Müllen, *Adv. Mater.* **2020**, 32, 2001893; d) A. V. Savin, *Phys. Solid State* **2018**, 60, 1046.
- [2] O. Gröning, S. Wang, X. Yao, C. A. Pignedoli, G. Borin Barin, C. Daniels, A. Cupo, V. Meunier, X. Feng, A. Narita, K. Müllen, P. Ruffieux, R. Fasel, *Nature* **2018**, 560, 209.
- [3] D. J. Rizzo, G. Veber, T. Cao, C. Bronner, T. Chen, F. Zhao, H. Rodriguez, S. G. Louie, M. F. Crommie, F. R. Fischer, *Nature* **2018**, 560, 204.
- [4] G. S. Diniz, G. I. Luiz, A. Latgé, E. Vernek, *Phys. Rev. B* **2018**, 97, 115444.
- [5] Q. Sun, X. Yao, O. Gröning, K. Eimre, C. A. Pignedoli, K. Müllen, A. Narita, R. Fasel, P. Ruffieux, *Nano Lett.* **2020**, 20, 6429.
- [6] S. Šćepanović, A. Kimouche, J. Mirković, G. Sadić, T. Klamroth, A. Hassanien, *Sci. Rep.* **2024**, 14, 11641.
- [7] X. Xu, K. Sun, A. Ishikawa, A. Narita, S. Kawai, *Angew. Chem., Int. Ed.* **2023**, 62, e202302534.
- [8] R. Yin, Z. Wang, S. Tan, C. Ma, B. Wang, *ACS Nano* **2023**, 17, 17610.
- [9] B. C. Stipe, M. A. Rezaei, W. Ho, *Science* **1998**, 280, 1732.
- [10] J. van der Lit, M. P. Boneschanscher, D. Vanmaekelbergh, M. Ijäs, A. Uppstu, M. Ervasti, A. Harju, P. Liljeroth, I. Swart, *Nat. Commun.* **2013**, 4, 2023.
- [11] C.-L. Chiang, C. Xu, Z. Han, W. Ho, *Science* **2014**, 344, 885.
- [12] A. Hassanien, *Phys. Status Solidi* **2024**, 18, 2400192.
- [13] E. E. Vdovin, K. Kapralov, Y. N. Khanin, A. Margaryan, K. Watanabe, T. Taniguchi, C. Yang, S. V. Morozov, D. A. Svintsov, K. S. Novoselov, D. A. Ghazaryan, *NPJ 2D Mater. Appl.* **2025**, 9, 7.

- [14] J. Overbeck, G. B. Barin, C. Daniels, M. L. Perrin, O. Braun, Q. Sun, R. Darawish, M. De Luca, X.-Y. Wang, T. Dumschlaff, A. Narita, K. Müllen, P. Ruffieux, V. Meunier, R. Fasel, M. Calame, *ACS Nano* **2019**, 13, 13083.
- [15] J. Cai, P. Ruffieux, R. Jaafar, M. Bieri, T. Braun, S. Blankenburg, M. Muoth, A. P. Seitsonen, M. Saleh, X. Feng, K. Müllen, R. Fasel, *Nature* **2010**, 466, 470.
- [16] I. Horcas, R. Fernández, J. M. Gómez-Rodríguez, J. Colchero, J. Gómez-Herrero, A. M. Baro, *Rev. Sci. Instrum.* **2007**, 78, 013705.
- [17] H. Huang, D. Wei, J. Sun, S. L. Wong, Y. P. Feng, A. H. C. Neto, A. T. S. Wee, *Sci. Rep.* **2012**, 2, 983.
- [18] O. Deniz, C. Sánchez-Sánchez, T. Dumschlaff, X. Feng, A. Narita, K. Müllen, N. Kharche, V. Meunier, R. Fasel, P. Ruffieux, *Nano Lett.* **2017**, 17, 2197.
- [19] H. Sevincli, M. Brandbyge, *Appl. Phys. Lett.* **2014**, 105, 153108.
- [20] E. E. Vdovin, A. Mishchenko, M. T. Greenaway, M. J. Zhu, D. Ghazaryan, A. Misra, Y. Cao, S. V. Morozov, O. Makarovskiy, T. M. Fromhold, A. Patané, G. J. Slotman, M. I. Katsnelson, A. K. Geim, K. S. Novoselov, L. Eaves, *Phys. Rev. Lett.* **2016**, 116, 186603.
- [21] D. Liu, C. Daniels, V. Meunier, A. G. Every, D. Tománek, *Carbon* **2020**, 157, 364.
- [22] T. Tanaka, A. Tajima, R. Moriizumi, M. Hosoda, R. Ohno, E. Rokuta, C. Oshima, S. Otani, *Solid State Commun.* **2002**, 123, 33.
- [23] L. M. Malard, M. A. Pimenta, G. Dresselhaus, M. S. Dresselhaus, *Phys. Rep.* **2009**, 473, 51.
- [24] J. Yan, T. Villarsen, E. A. Henriksen, P. Kim, A. Pinczuk, *Phys. Rev. B* **2009**, 80, 241417.
- [25] C. Ma, L. Liang, Z. Xiao, A. A. Puretzky, K. Hong, W. Lu, V. Meunier, J. Bernholc, A.-P. Li, *Nano Lett.* **2017**, 17, 6241.
- [26] a) M. Vandescuren, P. Hermet, V. Meunier, L. Henrard, P. Lambin, *Phys. Rev. B: Condens. Matter Mater. Phys.* **2008**, 78, 195401; b) H. Ishii, N. Kobayashi, K. Hirose, *Appl. Phys. Express* **2010**, 3, 095102; c) A. V. Savin, *Phys. Solid State* **2018**, 60, 1046.